Mixing and reaction fronts in laminar flows

Cite as: J. Chem. Phys. **120**, 7314 (2004); https://doi.org/10.1063/1.1665555
Submitted: 11 December 2003 • Accepted: 12 January 2004 • Published Online: 05 April 2004

M. Leconte, J. Martin, N. Rakotomalala, et al.

Mixing and reaction fronts in laminar flows

M. Leconte, J. Martin, N. Rakotomalala, and D. Salin
Laboratoire Fluides Automatique et Systèmes Thermiques, Universités P. et M. Curie and Paris Sud, C.N.R.S. (UMR7608), Bâtiment 502, Campus Universitaire, 91405 Orsay Cedex, France

Y. C. Yortsos
Department of Chemical Engineering, University of Southern California, Los Angeles, California 90089-1211

(Received 11 December 2003; accepted 12 January 2004)

Autocatalytic reaction fronts between unreacted and reacted mixtures in the absence of fluid flow propagate as solitary waves. In the presence of imposed flow, the interplay between diffusion and advection enhances the mixing, leading to Taylor hydrodynamic dispersion. We present asymptotic theories in the two limits of small and large Thiele modulus (slow and fast reaction kinetics, respectively) that incorporate flow, diffusion, and reaction. For the first case, we show that the problem can be handled to leading order by the introduction of the Taylor dispersion replacing the molecular diffusion coefficient by its Taylor counterpart. In the second case, the leading-order behavior satisfies the eikonal equation. Numerical simulations using a lattice gas model show good agreement with the theory. The Taylor model is relevant to microfluidics applications, whereas the eikonal model applies at larger length scales. © *2004 American Institute of Physics.*
[DOI: 10.1063/1.1665555]

INTRODUCTION

Interface motion and front propagation occur in many different areas, including chemical reactions,[1] atmospheric chemistry (ozone hole), population dynamics in biology,[2,3] and flame propagation in combustion.[4] Depending on the reaction kinetics, chemical reaction fronts exhibit fascinating phenomena such as Turing patterns, Belousov–Zhabotinsky oscillations, and chaotic or solitary wave propagation.[1] Autocatalytic reaction fronts between unreacted and reacted mixtures propagate as solitary waves at a constant velocity and with a stationary concentration profile.[5,6] A key issue in these problems is the selection of the front velocity. The problem was addressed long ago, but only a small number of cases are fully understood, among which are the celebrated and pioneering works of Fisher[2] and Kolmogorov–Petrovskii–Piskunov[3] (F-KPP),[1,4,7] with second-order kinetics. In contrast to flame propagation in combustion,[8] where it has been analyzed thoroughly theoretically and experimentally, the effect of fluid flow (laminar or turbulent) has not been explored in much detail in autocatalytic fronts until very recently.[9–15] Even then, many issues remain unresolved.

The specific objective of this paper is to analyze the effect of a laminar and spatially sinusoidal flow on autocatalytic reaction fronts. We will focus on two asymptotic limits, which admit an analytical description. At relatively slow kinetics, Taylor-like dispersion[16] dominates. The interplay between diffusion and advection enhances the mixing of the fluids species and leads to an overall macroscopic diffusion, known as Taylor hydrodynamic dispersion.[16] Therefore, when advection, reaction, and diffusion act together, one expects that the effective hydrodynamic mixing could change the overall diffusivity, leading to a different propagation velocity than that obtained in the absence of flow. Following Taylor's approach, we will derive here the corresponding asymptotics, considering specifically a spatially sinusoidal velocity profile. In the other limit of fast kinetics, the eikonal-equation regime applies, which has been extensively described.[10–14] To probe the validity of the asymptotic theories we subsequently perform numerical simulations based on the lattice Bhatnagar–Gross–Krook (BGK) method.[13,17] The iodate–arsenous-acid autocatalytic reaction[6,18] (IAA) is considered. Numerical and theoretical results are then compared and found to be in good agreement.

PRELIMINARIES

Consider a fluid containing an autocatalytic species. The fluid is advected with an imposed velocity. The mass balance for the reacting species is the advection–diffusion–reaction equation[17] (ADR)

$$\frac{\partial C}{\partial t}+\vec{U}\cdot\vec{\nabla}C=D_m\Delta C+\alpha f(C), \tag{1}$$

where C is a normalized concentration of the autocatalytic reactant, $\vec{U}$ the fluid velocity, D_m the molecular diffusion coefficient, α the kinetic parameter of the reaction rate, and $f(C)$ the functional dependence of the rate on concentration. We will assume that the viscosity and density of the fluid do not depend on the concentration (passive reacting species). Moreover, we will assume that the flow is steady and laminar, and without loss, unidirectional in the x direction. In two dimensions (2D), which will be the focus of the work from now on, Eq. (1) becomes

$$\frac{\partial C}{\partial t}+U(y)\frac{\partial C}{\partial x}=D_m\left(\frac{\partial^2 C}{\partial x^2}+\frac{\partial^2 C}{\partial y^2}\right)+\alpha f(C). \tag{2}$$

Consider now a problem in which a fluid of concentration 1 is injected into a medium with initial concentration 0.

In the absence of flow ($U=0$), Eq. (2) admits a one-dimensional stationary wave solution, propagating along the x direction with velocity V_χ. In the frame of reference moving at this velocity V_χ ($X=x-V_\chi t$), the traveling wave satisfies the following equation:

$$-V_\chi \frac{dC}{dX} = D_m \frac{d^2C}{dX^2} + \alpha f(C), \tag{3}$$

the order of which can be further reduced by 1. The particular value of V_χ depends sensitively on the kinetics. However, general bounds were also derived[7] for the general case

$$2\sqrt{\alpha D_m f'(0)} \leqslant V_\chi \leqslant 2\sqrt{\alpha D_m \sup_{C\in[0;1]} [f(C)/C]}. \tag{4}$$

Interestingly, for the Fisher–Kolmogorov–Petrovskii–Piskunov model, $f(C)$ is a convex function,[2,3] and the two bounds merge, leading to the explicit value for the velocity of the solitary wave, $V_\chi = 2\sqrt{\alpha D_m f'(0)}$. For our reaction involving iodate arsenous acid, the appropriate kinetic model is third order, $f(C)=C^2(1-C)$.[6,17,18] The particular kinetics leads to concentration profile $C(x,t)$, wave velocity V_χ, and characteristic front width l_χ, given by the following:

$$C(x,t) = \frac{1}{1+\exp[(x-V_\chi t)/l_\chi]},$$

$$V_\chi = \sqrt{\frac{\alpha D_m}{2}}, \tag{5}$$

$$l_\chi = \sqrt{\frac{2D_m}{\alpha}}.$$

Note that the above expression for the velocity also fulfills Eq. (4): $0 \leqslant V_\chi \leqslant \sqrt{\alpha D_m}$. The front width and velocity express the balance between diffusion and reaction, as the characteristic times for diffusion across the front (l_χ^2/D_m), reaction (α^{-1}), and the resulting propagation (l_χ/V_χ) are all comparable.

In the absence of chemical reaction ($\alpha=0$), Eq. (2) reduces to an advection–diffusion equation, which at the macroscale leads to hydrodynamic dispersion.[16] Tracer particles transported along the steady streamlines of a laminar velocity field can change streamlines, due to molecular diffusion. The concentration, averaged over a distance b transversely to the mean flow direction, is advected at the mean velocity $\bar{U}$ of the flow, but spreads in the flow direction at a rate faster than molecular diffusion alone, due to the different velocities along the different streamlines. This enhanced dispersion is the Taylor regime, which requires a concentration field almost homogeneous in the transverse direction. For a passive tracer, this is reached when the characteristic transverse diffusion time $\tau_{D_m} \sim b^2/D_m$ is sufficiently small compared to the advective time τ_{ad} which depends on the distance traveled L: $\tau_{ad} \sim L/\bar{U}$. The above requirement becomes one of small Peclet number, $\mathrm{Pe} = \bar{U}b/D_m < L/b$. In the Taylor regime, the average concentration $\bar{C}$ spreads in space and time following a "macroscopic" advection–diffusion equation with velocity $\bar{U}$ and effective diffusion coefficient D_{eff}:

$$\frac{\partial \bar{C}}{\partial t} + \bar{U}\frac{\partial \bar{C}}{\partial x} = D_{\mathrm{eff}} \frac{\partial^2 \bar{C}}{\partial x^2}, \tag{6}$$

where $D_{\mathrm{eff}} = D_m + D_T$ includes the Taylor regime contribution D_T. For a Haagen–Poiseuille (parabolic) type flow between two parallel plates separated by a small gap b, D_T is given by $D_T = \bar{U}^2 b^2/210 D_m$.[16]

In the presence of all three effects ($U\neq 0$, $\alpha\neq 0$, and $\mathrm{Pe} = \bar{U}b/D_m < L/b$), an increase of the diffusive transport is expected. Then, both the propagation velocity and the width of the front, which vary with the square root of the diffusion coefficient in the absence of flow [Eq. (5)], may increase accordingly. To study the interaction between the three effects, it is convenient to use the dimensionless Thiele modulus $\Phi^2 = \alpha b^2/D_m = 2(b/l_\chi)^2$. This number expresses the relative magnitude of the diffusion time to the reaction time and, in the present case, that of the spatial geometrical scale to the chemical one. We also note that Φ^2 is the product of the Peclet number with Damköhler number $\mathrm{Da} = \alpha b/\bar{U}$, which compares the advective time over distance b with the reaction time—namely, $\Phi^2 = \mathrm{Pe\,Da}$.[19] The effect of flow on chemical front propagation has already been addressed in certain asymptotic regimes: The studies in Refs. 9, 14, and 15 addressed the issue of small $\bar{U}$ compared to V_χ, leading to a second-order correction of the wave velocity; the study in Ref. 10 addressed the issue of a high flow rate, while Ref. 11 introduced, under slow reaction conditions, an upper bound to the front velocity, by replacing in Eq. (4) the molecular diffusion by its Taylor counterpart D_T. The case of third-order kinetics for a 2D flow between two parallel plates was addressed by Refs. 12 and 14 in the following regimes: a small velocity and/or small gap to first order and also a very large gap. The latter regime, corresponding to the eikonal model, has been often analyzed theoretically[10–12,14] and experimentally.[13]

As discussed above, in this work we will discuss the two different limits of small and large Thiele modulus, corresponding effectively to the Taylor and the eikonal regimes. The results will then be compared to numerical solutions obtained using a Lattice BGK method.

TAYLOR-LIKE APPROACH FOR ADVECTION DIFFUSION AND REACTION

Consider a steady-state propagation of concentration in a coordinate system moving with the front velocity V_f, in the presence of fluid flow. We have

$$[U(y)-V_f]\frac{\partial C}{\partial X} = D_m\left(\frac{\partial^2 C}{\partial X^2} + \frac{\partial^2 C}{\partial y^2}\right) + \alpha f(C), \tag{7}$$

where $X = x - V_f t$ is the coordinate in the moving frame. As is conventional for upscaling purposes, we express the concentration $C(X,y)$ and the velocity field $U(y)$ in terms of transversely averaged concentration $\bar{C}(X)$ and velocity $\bar{U}$, respectively:

$$C(X,y)=\overline{C}(X)+c(X,y), \quad U(y)=\overline{U}+u(y), \tag{8}$$

where $c(X,y)$ and $u(y)$ denote deviations from the mean. We noted above that in the Taylor regime, the concentration is assumed to be almost uniform transversely; hence c represents a small departure from the average: $c \ll \overline{C}$. Use of these expressions in Eq. (7) leads to first order in c to the following:

$$(\overline{U}-V_f+u)\left(\frac{d\overline{C}}{dX}+\frac{\partial c}{\partial X}\right)=D_m\left(\frac{d^2\overline{C}}{dX^2}+\frac{\partial^2 c}{\partial X^2}+\frac{\partial^2 c}{\partial y^2}\right)+\alpha[f(\overline{C})+cf'(\overline{C})], \tag{9}$$

the transverse averaging of which is

$$(\overline{U}-V_f)\frac{d\overline{C}}{dX}=-\frac{\partial \overline{uc}}{\partial X}+D_m\frac{d^2\overline{C}}{dX^2}+\alpha f(\overline{C}). \tag{10}$$

The vanishing of the average of $\partial^2 c/\partial y^2$ is due to either no-flux or periodic boundary conditions. To obtain $\overline{C}$ from Eq. (10), the flux $\overline{uc}$ and hence the deviation c from the mean are needed. The solution for c is obtained by substracting the equation for the average concentration [Eq. (10)] from that of the total concentration [Eq. (9)], thus yielding

$$(\overline{U}-V_f+u)\frac{\partial c}{\partial X}+u\frac{d\overline{C}}{dX}=\frac{\partial \overline{uc}}{\partial X}+D_m\left(\frac{\partial^2 c}{\partial X^2}+\frac{\partial^2 c}{\partial y^2}\right)+\alpha c f'(\overline{C}). \tag{11}$$

Next, we assume, as is conventional in these problems, that the variation of c along the flow direction X is negligible, thus obtaining the following differential equation for c:

$$u\frac{d\overline{C}}{dX}=D_m\frac{\partial^2 c}{\partial y^2}+\alpha c f'(\overline{C}). \tag{12}$$

Under the previous assumptions, this equation shows that c can be expressed in the form

$$c(X,y)=h(y)\frac{d\overline{C}}{dX}, \tag{13}$$

where $h(y)$ obeys the differential equation:

$$D_m h''(y)+\alpha f'(\overline{C})h(y)=u(y). \tag{14}$$

The flux $\overline{uc}$, across the plane moving at velocity V_f, is, therefore, Fickian and reads

$$\overline{uc}=-D_{T\chi}\frac{d\overline{C}}{dX}. \tag{15}$$

The proportionality coefficient $D_{T\chi}=-\overline{uh}$ depends on $\overline{C}$, α, u, D_m, and b. It follows that the upscaled equation for $\overline{C}$ [Eq. (10)] reads

$$(\overline{U}-V_f)\frac{d\overline{C}}{dX}=\frac{d}{dX}\left[(D_m+D_{T\chi})\frac{d\overline{C}}{dX}\right]+\alpha f(\overline{C}). \tag{16}$$

Under the approximations made, the upscaled equation (16) differs from Eq. (3) only by the diffusion coefficient $D_m+D_{T\chi}$ (instead of D_m). However, because of the concentration dependence of $D_{T\chi}$, the equation is one of nonlinear diffusion: $D_{\text{eff}}(\overline{C})=D_m+D_{T\chi}(\overline{C})$. Nonetheless, as the $\overline{C}$ dependence of $D_{T\chi}$ comes from the chemical term in Eq. (14), it is not difficult to show that this dependence can be neglected when the Thiele modulus is small, $\Phi^2=\alpha b^2/D_m \ll 1$. In this case, the Taylor regime condition $c \ll \overline{C}$ reduces to Pe $\Phi \ll 1$, the diffusion across the transverse direction is fast compared to the convection along the reaction front ($\tau_{D_m} < \tau_{ad}=l_\chi/V_\chi$). Under these conditions, we have simply Taylor diffusion—namely, $D_{\text{eff}}=D_m+D_T$—and the solution of Eq. (16) is a traveling wave, with velocity V_f bounded according to Eq. (4) and where D_m must be replaced by D_{eff}, as also suggested in Ref. 11.

For the third-order kinetics function $f(C)=C^2(1-C)$, the solution for $\overline{C}$ in the regime Pe $\Phi \ll 1$ and $\Phi^2 \ll 1$ is given by Eq. (5), where the velocity and width of the front are equal to

$$V_f=\overline{U}+\sqrt{\frac{\alpha(D_m+D_T)}{2}}=\overline{U}+V_\chi\sqrt{1+\frac{D_T}{D_m}}, \qquad l_{\text{eff}}=\sqrt{\frac{2(D_m+D_T)}{\alpha}}=l_\chi\sqrt{1+\frac{D_T}{D_m}}. \tag{17}$$

From Taylor's theory, D_T/D_m can be expressed in terms of the normalized average flow velocity $\epsilon=\overline{U}/V_\chi$, since $D_T/D_m=a\text{Pe}^2=a'\epsilon^2$, where a is the geometrical factor involved in Taylor dispersion, $a'=a(V_\chi b/D_m)^2$. Therefore, in the limit Pe $\ll 1$, the normalized front velocity behaves like $V_f/V_\chi \simeq 1+\epsilon+a'\epsilon^2/2$, in accordance with Refs. 9 and 14.

As an illustration, we will focus in the following on the sinusoidal velocity profile $U(y)=u(y)=U_M \sin(ky)$, where k is the wave vector of the sinusoidal perturbation. This has the advantage of zero mean flow and also emphasizes Taylor dispersion effects. The solution of the differential equation for $h(y)$ [Eq. (14)] and the calculation of $D_{T\chi}=-\overline{uh}$ are, respectively,

$$h(y)=-\frac{\text{Pe}}{1-f'(\overline{C})\Phi^2}\frac{\sin(ky)}{k}, \qquad D_{T\chi}=\frac{\text{Pe}^2}{1-f'(\overline{C})\Phi^2}\frac{D_m}{2}, \tag{18}$$

where we have also used the following dimensionless numbers:

$$\epsilon=\frac{U_M}{V_\chi}, \qquad \text{Pe}=\frac{U_M}{kD_m}=\frac{\epsilon}{kl_\chi}, \qquad \Phi^2=\frac{\alpha}{D_m k^2}=\frac{2}{(kl_\chi)^2}. \tag{19}$$

Analogous expressions for Poiseuille flow are given in the Appendix. Clearly, when the Thiele modulus is small, $\Phi^2 \ll 1$, the diffusion coefficient $D_{T\chi}$ reduces to $D_T=\text{Pe}^2 D_m/2$, leading to the same normalized front velocity and width, equal to

$$\frac{V_f}{V_\chi}=\frac{l_{\text{eff}}}{l_\chi}=\sqrt{1+\frac{\text{Pe}^2}{2}}. \tag{20}$$

This expression shows that the correction to the chemical wave velocity is a pure Taylor dispersion one. Moreover, in the limit $\text{Pe}\ll 1$, the normalized front velocity takes the form $V_f/V_\chi \simeq 1+\text{Pe}^2/4$, as also proposed in Ref. 9.

EIKONAL REGIME

The opposite limit corresponds to large Φ^2 values, and it is described by the eikonal equation, which has been extensively studied.[10–14] When $\Phi\to\infty$, diffusion has an effect on a very small scale, compared to the external length scale—for example, the wavelength of the velocity field. In this case, the velocity and shape of the front are linked together through the eikonal equation[12–14]

$$\vec{V}_f\cdot\vec{n}=V_\chi+\vec{U}\cdot\vec{n}+D_m\kappa. \tag{21}$$

Here, $\vec{n}$ is the unit vector normal to the front profile (oriented from $C=0$ to $C=1$), $\vec{U}$ is the imposed flow velocity, and κ is the front curvature. Neglecting the local front curvature and considering the unidirectional imposed flow, the eikonal equation reads

$$V_f=V_\chi/\cos\beta+U(y), \tag{22}$$

where β is the angle between $\vec{n}$ and the front velocity vector. Given V_f, one can solve Eq. (22) for the front shape. Results will be shown below.

LATTICE BGK SIMULATIONS

We used Lattice BGK methods[13,17,20,21] to simulate the solution of Eq. (1), using periodic boundary conditions on the transverse y direction. A periodic stationary velocity field $U(y)=U_M\sin(ky)$ was applied, where the wavelength $\lambda=2\pi/k$ is equal to the lattice width. In the specific simulations, the velocity V_χ and width of the front, l_χ, were taken equal to 0.016 and 8, respectively. We used as control parameters the normalized velocity $\epsilon=U_M/V_\chi$ and the normalized wave vector kl_χ or, equivalently, the Thiele modulus $\Phi^2=2/(kl_\chi)^2$. The Peclet number may then be expressed as $\text{Pe}=\epsilon\Phi/\sqrt{2}$. The numerical simulations were performed on lattices of typical length 2000 and of a width λ ranging between 24 and 160.

Figure 1 displays the time evolution of the propagation velocities of three different values of the average concentration ($\bar{C}=0.3$, 0.5, and 0.7). We note that within a time interval of the order of λ/V_χ all values reach the same asymptotic velocity, V_f, beyond which the front shape becomes stationary. The traveling-wave-averaged concentration profiles $\bar{C}(x)$ are shown in Fig. 2, for various values of the control parameters ϵ and Φ^2. In the figure, the value of Pe Φ increases in the direction from top to bottom. There is an increasing deviation of the profile from the predictions from Eq. (5), as the product increases, and for higher values of Φ, in accordance with the above-mentioned Taylor regime condition $\text{Pe}\,\Phi\ll 1$. It is interesting to note that the profile obtained at the largest ϵ and Φ values is characterized by two inflexion points. In the following, we will refer to this type of profiles as distorted.

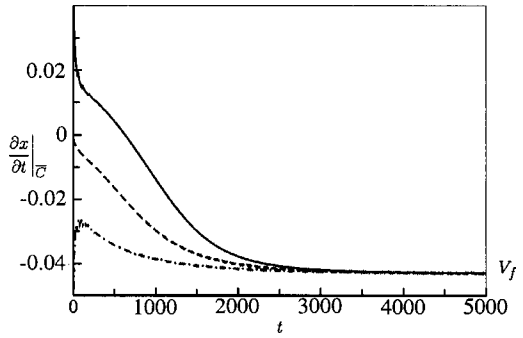

FIG. 1. Time evolution of the velocity of three averaged concentration values toward the asymptotic velocity V_f of the traveling wave, for $\Phi^2=3.24$ and $\epsilon=3$. Solid line: $\bar{C}=0.7$. Dashed line: $\bar{C}=0.5$. Dot-dashed line: $\bar{C}=0.3$.

Figure 3 shows numerical results for the normalized front extent l_{eff}/l_χ as a function of the Peclet number for different values of the Thiele modulus. The value of $(l_{\text{eff}}/l_\chi)^2$ was obtained by the ratio of the second-order moment of the derivative of the numerical concentration profile over the one of the analytical concentration profile given by Eq. (5) ($\pi^2 l_{\text{eff}}^2/3$). The theoretical predictions from Eq. (20) are also plotted. There is good agreement between theory and simulations for the smaller values of the Thiele modulus, as expected. The agreement holds for Pe Φ values up to 1.67 (corresponding to $\text{Pe}\simeq 2.5$). For the larger value $\Phi^2=3.24>1$, the agreement is surprisingly good for Pe $\Phi\simeq 1.2$ (corresponding to $\text{Pe}\simeq 0.7$). Above this value, the profiles become distorted, but their width is close to the theoretical prediction, up to Pe $\Phi\simeq 6$ ($\text{Pe}\simeq 3.5$). Figure 4 displays the front velocity, normalized by V_χ, versus the Peclet number, for two values of Φ^2 from Fig. 3. Surprisingly, for $\Phi^2=0.45$, the agreement with the theoretical prediction from Eq. (20) holds over the entire range of Pe (up to $\text{Pe}\simeq 10$, Pe $\Phi\simeq 6.7$). For $\Phi^2=3.24$, the front velocity is overpredicted by Eq. (20) as Pe (or Pe Φ) increases above the value of 1, where the profiles become distorted.

We recall that Eq. (20) was derived under the two assumptions $\Phi^2\ll 1$ and $\epsilon\Phi^2\ll 1$ (or Pe $\Phi\ll 1$). Thus, the domain of validity of the Taylor regime is expected to be delineated, in a $\epsilon(\Phi)$ diagram, by the curves $\Phi=1$, $\epsilon\Phi^2=1$, and the two axes $\epsilon=0$ and $\Phi=0$, as shown in Fig. 5. Note that the axis $\epsilon=0$ is included, as Eq. (20) still holds in the absence of flow, but the axis $\Phi=0$ is excluded, as it does not correspond to the propagation of a solitary wave but to the pure Taylor diffusive process (in which no stationary extension can be defined). The numerical results are also shown in Fig. 5. Solid circles denote agreement, the $\times$ symbols denote departure from Taylor regime predictions (based on an arbitrary relative error of 5%).

It is shown that the validity of Eq. (20) is quite good in the region of the parameter space under the curve $\epsilon\Phi^2=1$, and even sligthly above. The arbitrary criterion used corresponds in fact to the parameter $\epsilon\Phi^2$ being less than several units. Surprisingly enough, this last condition is found to be

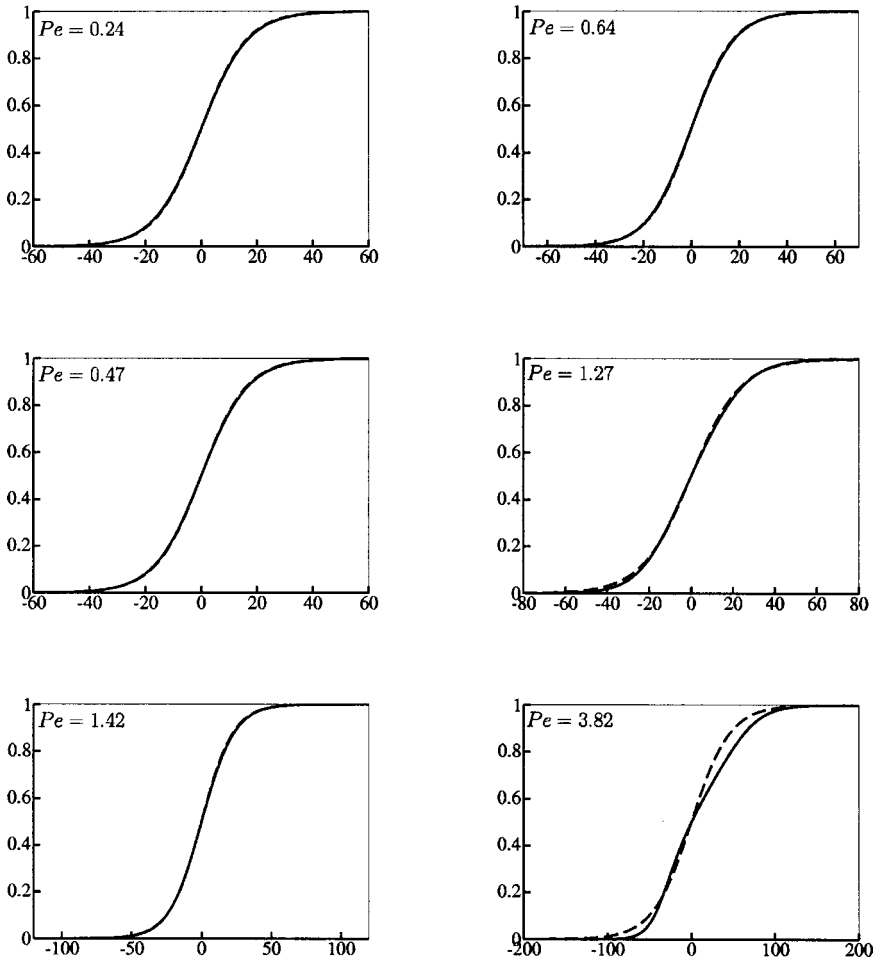

FIG. 2. Averaged concentration profiles in the stationary state. Solid line: numerical simulations. Dashed line: theoretical results from Eq. (5). Left column: $\Phi^2=0.45$. Right column: $\Phi^2=3.24$. From top to bottom, the normalized flow velocity ϵ takes the values 0.5, 1, 3, respectively. Also shown is the corresponding Peclet number.

sufficient, for the Taylor regime predictions to apply, over the whole range of Φ explored numerically (up to $\Phi\simeq 6.3$—i.e., $\Phi^2\simeq 40$). This suggests that the condition $\Phi^2\ll 1$, which was needed to approximate the nonlinear diffusivity $D_{T\chi}$ by its linear counterpart $D_T=\mathrm{Pe}^2 D_m/2$, is not necessary for Eq. (20) to apply. This is all the more unexpected since for our kinetics reaction function $f(C)=C^2(1-C)$, the denominator of $D_{T\chi}$ [Eq. (18)], $1-f'(C)\Phi^2$, has two real roots between 0 and 1, for all Φ^2 values greater than 3. Hence, provided that $\epsilon\Phi^2<1$, the local divergence of the nonlinear diffusivity $D_{T\chi}(C)$, for $\Phi^2>3$, does not appear to play any significant role in the propagation of the stationary front, and both extent and velocity can be approximated by Eq. (20). We remark, however, that in this domain ($\epsilon\Phi^2<1$ and $\Phi^2>3$) the Taylor counterpart D_T indicates only a second-order correction, and the front is hardly affected by flow.

In summary, the Taylor regime predictions [Eq. (20)] correctly account for a significant influence of the flow on the chemical front propagation, in the domain $\epsilon\Phi^2<1$ and $\Phi^2<1$. This last condition means that the extent of the front in the absence of flow ($l_\chi\simeq 100\,\mu$m for the IAA reaction) has to be larger than the transverse dimension λ of the flow

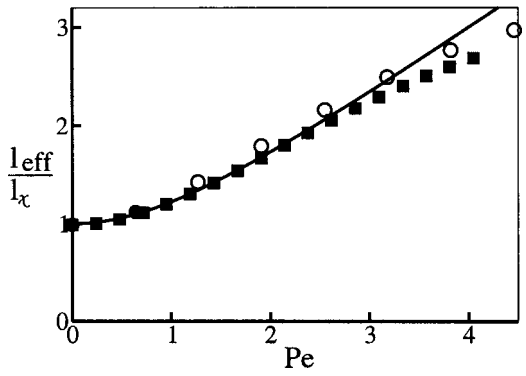

FIG. 3. Normalized front extent (l_f/l_χ) vs the Peclet number ($\mathrm{Pe}=U_m/V_\chi k l_\chi$). ■: $\Phi^2=0.45$, ●: $\Phi^2=3.24$, ○: $\Phi^2=3.24$ (distorted profile, cf. text). Solid line: pure Taylor expansion ($l_{\mathrm{eff}}/l_\chi=\sqrt{1+\mathrm{Pe}^2/2}$).

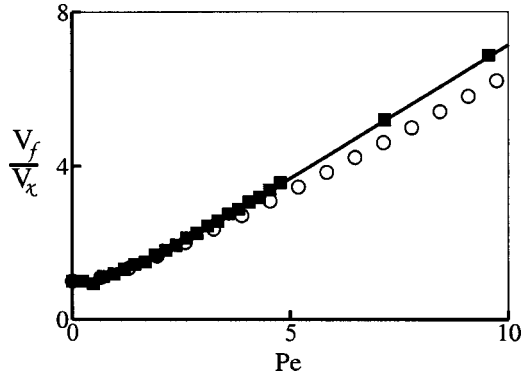

FIG. 4. Normalized front velocity (V_f/V_χ) vs the Peclet number ($\mathrm{Pe}=U_m/V_\chi k l_\chi$). ■: $\Phi^2=0.45$, ●: $\Phi^2=3.24$, ○: distorded profiles. Solid line: pure Taylor expansion.

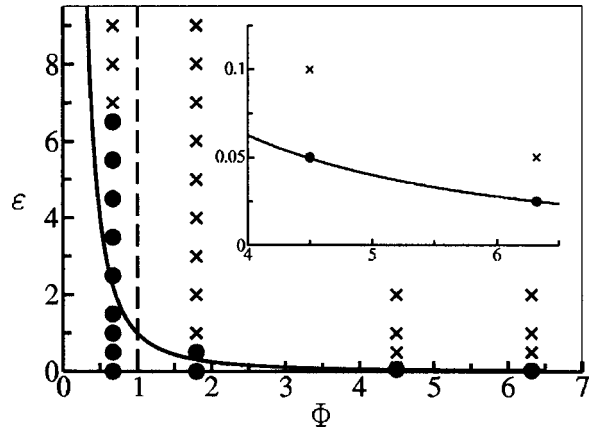

FIG. 5. Region of the validity of the Taylor regime in the parameter space. The solid line denotes the curve $\epsilon=1/\Phi^2$; the dashed line is the curve $\Phi=1$. Solid circles: simulations and Taylor regime predictions in agreement. ×: simulations and theory not in agreement. Inset: zoom-in for the smaller values of ϵ.

(or the cell). Hence, the Taylor regime applies to a range of flow velocities which increases as the transverse dimension of the system decreases, and for this reason it is likely to be relevant in microfluidic systems.

Before closing this part, we provide one more figure to illustrate the effect of the Thiele modulus on the concentration front. Figure 6 shows two isoconcentration contours $C=0.5$ and $C=0.4$ for several different values of the parameters ϵ and Φ. For a constant value of ϵ (left or right column), an increase in Φ (occurring from top to bottom in Fig. 6) leads to both a sharpening and distortion of the front. The concentration contours approach each other, as expected, and they also exhibit a departure from the sinusoidal shape. These features signal the approach of the profile towards the eikonal regime, which, unlike the Taylor regime, is dominated by the nonlinear effects.

Consider, now, the eikonal regime. A simulation of the front in this regime ($\epsilon=14.9$ and $\Phi^2\sim506$) is shown in Fig. 7. In agreement with Refs. 10–12, the front shape is not symmetric: while the head of the front (leading edge, low values of x in Fig. 7) is flatter (as compared to a sinusoidal), its back (trailing edge, higher values of x in Fig. 7) exhibits a cusp shape. It is interesting to plot the normalized front velocity V_f/V_χ versus the normalized maximum flow velocity $\epsilon=U_M/V_\chi$. The results are shown in Fig. 8. We find that V_f/V_χ tends to $1+\epsilon$ as ϵ increases, as expected.[12] This means that the front is advected at the maximum possible velocity (with $\epsilon>0$ on the right of Fig. 7), based on which the front shape can be determined; then the angle θ at the cusp is

$$1+\epsilon=\frac{1}{\cos\theta}-\epsilon, \tag{23}$$

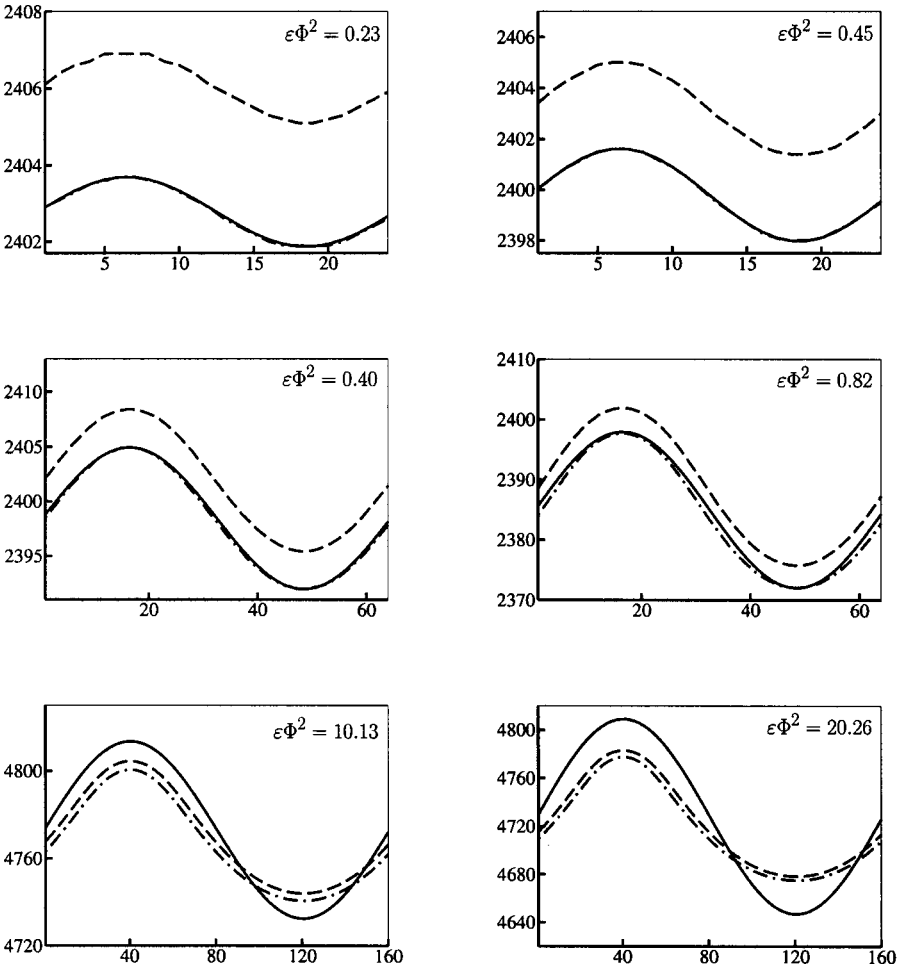

FIG. 6. Isoconcentration contours $C=0.4$ (dot-dashed line) and $C=0.5$ (dashed line) in the stationary state. Solid line: theoretical results expected in the Taylor regime [from Eq. (5)]. Left column: $\epsilon=0.5$, right column: $\epsilon=1$. From top to bottom: $\Phi^2=0.45$, 3.24, and 20.25.

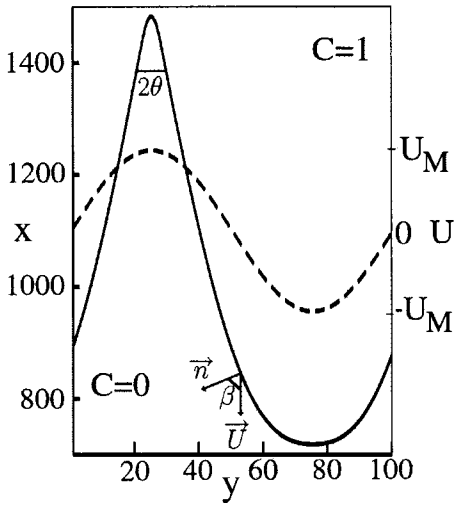

FIG. 7. Isoconcentration contour $C=0.5$ in the eikonal regime ($\epsilon=14.9$ and $\Phi^2=506$) and imposed velocity profile (dashed line, axis on the right). Note that the aspect ratio of the figure is not 1.

leading to the result $\cos\theta=1/(2\epsilon+1)$. This suggests that $\theta\to\pi/2$ when $\epsilon\to\infty$; that is, the front shape on the left side of Fig. 7 tends to a cusp when ϵ increases. Note also that our measurement of $\theta\sim0.03$ in Fig. 7 is in reasonable agreement with Eq. (23) which predicts $1/(2\epsilon+1)=0.03$ for $\epsilon=14.9$. To conclude, we plot in Fig. 9 the evolution of V_f/V_χ versus Φ^2. In agreement with the previous predictions, $V_f/V_\chi\to1+\epsilon$ when $\Phi^2\to\infty$ (eikonal regime for large Φ^2), and $V_f/V_\chi\sim\sqrt{1+\mathrm{Pe}^2/2}$ for $\Phi^2\to0$ (Taylor-like regime for Φ^2 less than 1).

CONCLUSIONS

In this paper, we presented a Taylor-like approach[16] for the development of an autocatalytic reaction front in the presence of a laminar velocity field, under conditions of slow kinetics. Analytical results were derived for the velocity and the extent of the concentration profile, in the asymptotic traveling wave solution. A correction to the purely chemical wave front arises from Taylor-like dispersion, which does not include any contribution of the chemical reaction in the limit of small Thiele modulus ($\Phi^2\leqslant1$) and small Peclet number

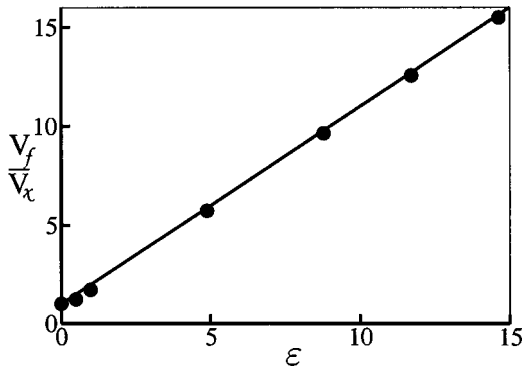

FIG. 8. Normalized front velocity V_f/V_χ versus ϵ in the eikonal regime ($\Phi^2=506$). ●: numerical simulations. Solid line: eikonal theoretical result, $V_f/V_\chi=1+\epsilon$.

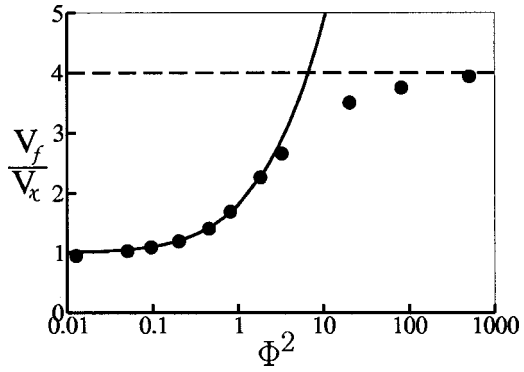

FIG. 9. Normalized front velocity V_f/V_χ versus Φ^2 for $\epsilon=3$, showing the transition between the Taylor regime (small Φ^2) and the eikonal regime (large Φ^2). ●: simulations. Solid line: pure Taylor expansion. Dashed line: eikonal approach.

(Pe $\Phi\leqslant1$). The opposite, eikonal, regime was also discussed. We tested our predictions using numerical lattice BGK simulations for third-order reaction kinetics, in the advection–diffusion–reaction equation, and with a sinusoidal variation of the velocity field. Good agreement was obtained between the simulations and the Taylor expansion, at small Φ, and the eikonal regime predictions at large Φ.

ACKNOWLEDGMENTS

This work benefited from discussions with Dr Böckmann. The research was partly supported by IDRIS (Project No. 034052), CNES No. 793/CNES/00/8368, and ESA (No. AO-99-083). All these sources of support are gratefully acknowledged.

APPENDIX: EFFECT OF A 2D HAAGEN-POISEUILLE FLOW ON THE FRONT VELOCITY

In this Appendix we provide results for the advection–diffusion–reaction equation corresponding to the following 2D Haagen–Poiseuille flow between two parallel boundaries located at $y=\pm b/2$:

$$U(Y)=6\overline{U}(1-Y)Y=\tfrac{3}{2}\overline{U}(1-X^2). \tag{A1}$$

Here, we denoted $Y=1/2+y/b=(1+X)/2$. To facilitate comparison with Refs. 12 and 14, we introduce the reduced velocity $\epsilon=\overline{U}/V_\chi$ and the reduced width $\eta=b/(2l_\chi)$, which is linked to the Thiele modulus for a third-order reaction, $\Phi^2=4\eta^2$.

Performing our Taylor-like expansion, with $u=U-\overline{U}$, we get the following expression for the front profile correction:

$$h(Y)=\frac{6\overline{U}b^2}{D_m z^2}\left(\frac{1}{6}-Y+Y^2+\frac{2}{z^2}-\frac{\cosh(Yz)\coth(z/2)}{z}+\frac{\sinh(Yz)}{z}\right), \tag{A2}$$

where $z^2=-\Phi^2 f'(\overline{C})$, and for the dispersion coefficient,

$$D_{T\chi}=\frac{\overline{U^2}b^2}{210D_m}G(z),$$

$$G(z)=\frac{210}{5z^6}[720+60z^2-z^4-360z\coth(z/2)]. \tag{A3}$$

Note that expression (A2) is valid for real or imaginary z. It is instructive to expand the above results in series of z (i.e., in terms of the Thiele modulus),

$$h(y)=\frac{\overline{U}b^2}{D_m}\left(\frac{1}{60}-\frac{Y^2}{2}(1-Y^2)+O(z^2)\right),$$

$$G(z)=1-\frac{z^2}{40}, \tag{A4}$$

which, after introducing ϵ and η, leads to

$$\frac{2h(X)}{b}=\frac{\epsilon\eta}{2}\left(\frac{X^2}{4}-\frac{X^4}{8}-\frac{13}{120}\right). \tag{A5}$$

This is exactly Spangler and Edward's result.[14] Likewise for dispersion and hence for the velocity correction using Eq. (17), we get

$$u=V_f/V_\chi=\sqrt{1+\frac{4\epsilon^2\eta^2}{210}G(z)}$$

$$\simeq 1+\epsilon+\frac{(\epsilon\eta)^2}{105}+O(z^2), \tag{A6}$$

again in agreement with Spangler and Edward's second-order expansion.

[1] S. K. Scott, *Oscillations, Waves and Chaos in Chemical Kinetics* (Oxford University Press, Oxford, 1994).
[2] R. A. Fisher, Proc. Annu. Symp. Eugen. Soc. **7**, 355 (1937).
[3] A. N. Kolmogorov, I. G. Petrovskii, and N. S. Piskunov, Moscow Univ. Math. Bull. (Engl. Transl.) **1**, 1 (1937).
[4] Ya. B. Zeldovitch and D. A. Franck-Kamenetskii, Actu. Phys. USSR. **9**, 341 (1938).
[5] P. A. Epik and N. S. Shub, Dokl. Akad. Nauk SSSR **100**, 503 (1955).
[6] A. Hanna, A. Saul, and K. Showalter, J. Am. Chem. Soc. **104**, 3838 (1982).
[7] U. Ebert and W. van Saarloos, Physica D **146**, 1 (2000).
[8] P. Clavin, Prog. Energy Combust. Sci. **11**, 1 (1985).
[9] G. Papanicolaou and J. Xin, J. Stat. Phys. **63**, 915 (1991).
[10] B. Audoly, H. Berestycki, and Y. Pomeau, C. R. Seances Acad. Sci., Ser. B **328**, 255 (2000).
[11] M. Abel, A. Celani, D. Vergni, and A. Vulpiani, Phys. Rev. E **64**, 046307 (2001).
[12] B. F. Edwards, Phys. Rev. Lett. **89**, 104501 (2002).
[13] M. Leconte, J. Martin, N. Rakotomalala, and D. Salin, Phys. Rev. Lett. **90**, 128302 (2003).
[14] R. S. Spangler and B. F. Edwards, J. Chem. Phys. **118**, 5911 (2003).
[15] J. Nolen and J. Xin, J. Multiscale Modeling Simul. **1**, 554 (2003).
[16] G. I. Taylor, Proc. R. Soc. London, Ser. A **219**, 186 (1953); Proc. R. Soc. London, Ser. B **67**, 857 (1954).
[17] J. Martin, N. Rakotomalala, D. Salin, and M. Böckmann, Phys. Rev. E **65**, 051605 (2002).
[18] M. Böckmann and S. C. Müller, Phys. Rev. Lett. **85**, 2506 (2000).
[19] P. E. Kechagia, I. N. Tsimpanogiannis, Y. C. Yortsos, and P. Lichtner, Chem. Eng. Sci. **57**, 2565 (2002).
[20] N. Rakotomalala, D. Salin, and P. Watzky, J. Fluid Mech. **338**, 277 (1997).
[21] P. Gondret, N. Rakotomalala, M. Rabaud, D. Salin, and P. Watzky, Phys. Fluids **9**, 1841 (1997).